PNAS
www.pnas.org

Supplementary Information for

Measuring the Effectiveness of High-Performance Co-Optima Biofuels on Suppressing Soot Formation at High Temperatures

Samuel Barak[1], Ramees Rahman[1], Sneha Neupane[1], Erik Ninnemann[1], Farhan Arafin[1], Andrew Laich[1], Anthony C. Terracciano[1], and Subith Vasu[1, 2].

[1]Center for Advanced Turbomachinery and Energy Research (CATER), Mechanical and Aerospace Engineering Department, University of Central Florida, 4000 Central Florida Blvd, Orlando, FL 32816, USA
[2]CREOL, The College of Optics and Photonics, University of Central Florida, 4000 Central Florida Blvd, Orlando, FL 32816, USA

Corresponding Author: Subith Vasu
Email: subith@ucf.edu

This PDF file includes:

Supplementary text
Figures S1 to S7
Tables S1 to S7
SI References

www.pnas.org/cgi/doi/10.1073/pnas.1920223117

Calibration of Soot Measurements

Obtaining soot measurements involved implementing several considerations from literature adapted to our facility (1-4). Mixtures (1) and (2) in Table 1 only contained ethylene as fuel. Experiments conducted using these mixtures ensure that our methods were valid and comparable to literature(1). Verified elements included our laser setup, experiment preparation, as well as experimental soot yields, and trends. We implemented to use an ethylene mixture standard as was done in other works with as little as possible variation (1). Our SY_E results were in-line with the results from this publication: in bell-shape, temperature range, and soot yield. We could not perform the same exact configuration as the other group because our shock tube has a larger diameter (and therefore longer pathlength). When we had attempted the same mixture, our absorbances were extremely large and useful data could not be gathered.

Reaction Pathways to Soot

To understand the formation of soot from the different biofuels, the gas-phase reaction pathways for each was investigated using the Co-Optima mechanism. This study will also give insights to additional pathways to be considered in future efforts.

Ethylene

Figure S1 illustrates the pathway of ethylene to benzene for mixture (2). Ethylene initially undergoes H-abstraction to form a C_2H_3 radical which then undergoes radical decomposition to form acetylene (C_2H_2). Acetylene then form the propargyl (C_3H_3) radical which then forms benzene (C_6H_6). The amount of benzene formed is highly dependent on total C_3H_3 produced. Hence another important pathway for C_3H_3 formation from C_2H_3 is also shown here. With the addition of biofuels into ethylene, these pathways play an important role in PAH growth and soot formation. In Fig. S1, the species highlighted in red will contribute to more benzene and hence more PAH and soot. Species shown in green are the result of oxidation and more of these species ensures that more of fuel is oxidized.

$$C_2H_4+H \Leftrightarrow C_2H_3+H_2$$
$$C_2H_3 \Leftrightarrow C_2H_2+H$$
$$C_2H_2+CH_2 \Leftrightarrow C_3H_3$$
$$C_3H_3+C_3H_3 \Leftrightarrow C_6H_6$$

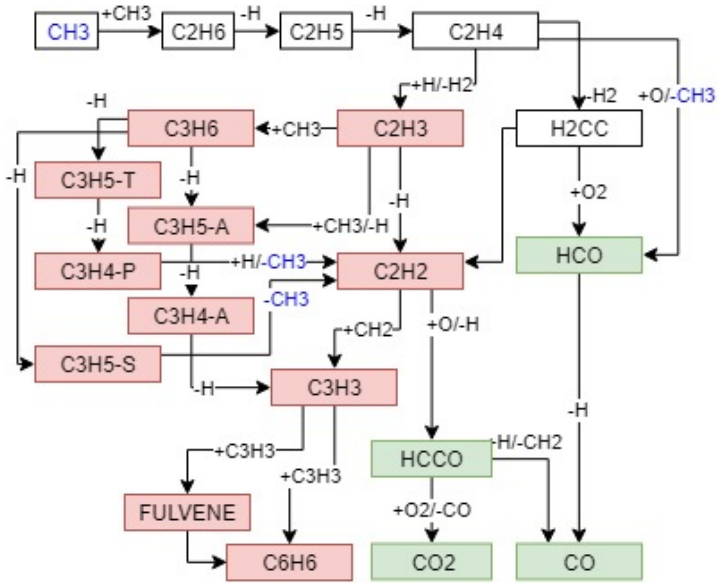

Figure S1. Pathway diagram showing ethylene at 1850 K and 4.5atm growth to benzene. Red highlights are species which act as key intermediates in formation of benzene and other polycyclic aromatic hydrocarbons. Species highlighted in green are directly related to oxidation pathway. Refer to the color version of this figure.

Ethylene also reacts with atomic oxygen to produce methyl radical (shown with blue font) which undergoes self-recombination to produce C_2H_6. C_2H_6 then loses hydrogen in sequential reactions to form ethylene and then proceeds to form benzene as shown in Fig. S1. Since there are many reactions which release methyl radicals in different biofuels considered in this work, this pathway plays a significant role in formation of benzene and soot precursors.

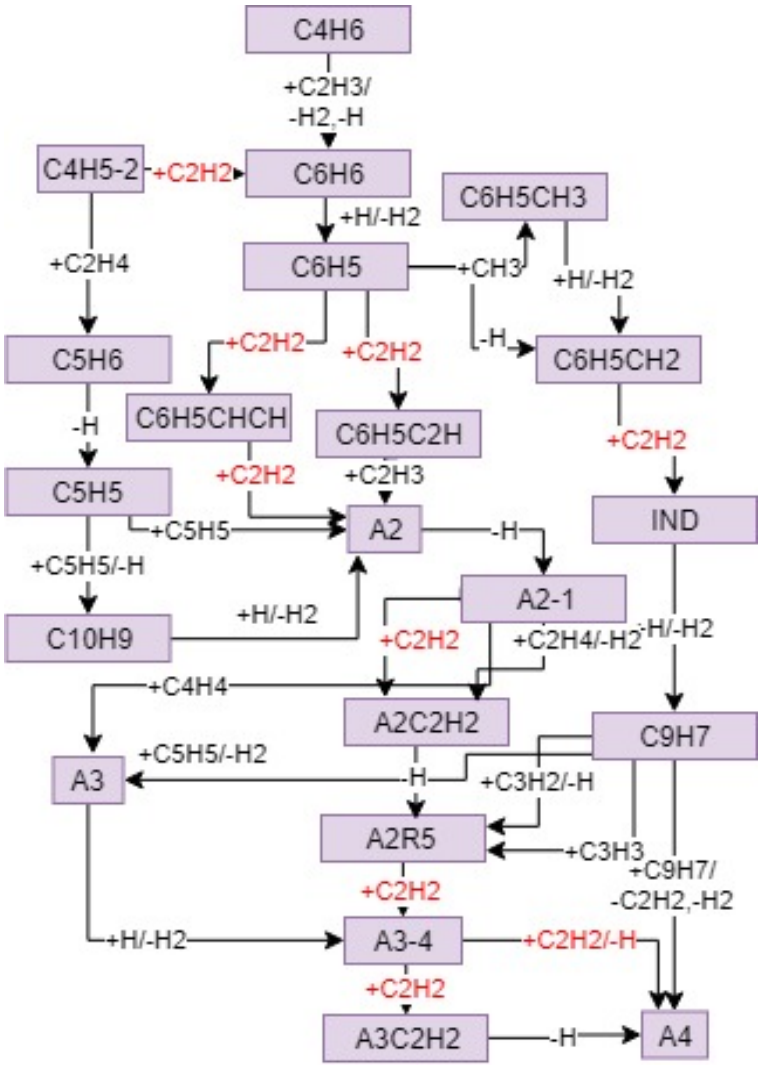

Figure S2. Pathway diagram showing important reactions for growth of benzene (C_6H_6) to pyrene (A4). Refer to the color version of this figure.

As the precursor for soot is benzene formation followed by polycyclic aromatic growth, the pathway is important. The Co-Optima mechanism did not include reactions enabling pyrene formation; therefore, reactions were taken from the KM2 mechanism until pyrene. Figure S2 shows key pathways for agglomerations of benzene into pyrene (A4). This mainly takes place through the C_2H_2 addition (highlighted red) following H abstraction of the parent benzene (HACA). Other dominant reactions for growth of PAHs include the reactions with C_3H_3, C_4H_4 and C_5H_5. Indenyl radical (C_9H_7), a resonance stabilized species, also plays an important role in PAH growth enabling pyrene formation directly from a self-recombination reaction. It also forms phenanthrene (A3) via an C_5H_5 addition reaction. The effect of these resonant stabilized radicals in PAH growth has been studied in many previous works (5, 6). Although Fig. S2 is for PAH formation from ethylene, the radicals and molecules contained within the reaction mechanisms will be present within the other

biofuel combustion and as a result also sheds insight to how those fuels may form PAHs and subsequently, soot.

Methylfuran

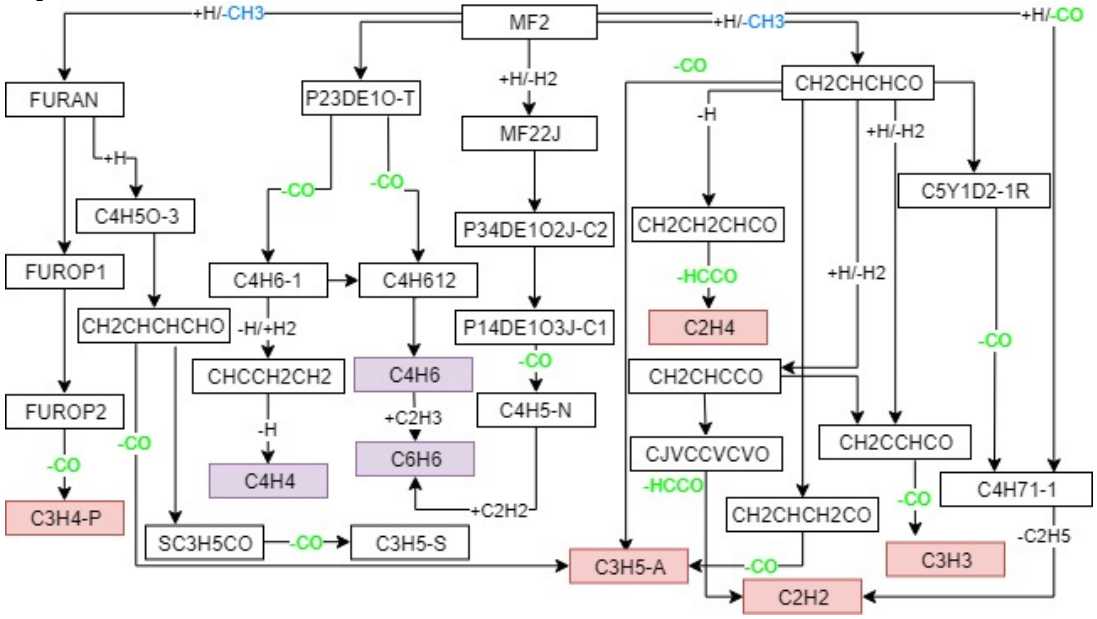

Figure S3. Reaction pathway for methylfuran at 1850K and 4.5 atm showing dominant reactions. Refer to the color version of this figure.

The decomposition of methyl furan initiates via a ring opening reaction forming 2,3-pentadienal (P23DE1O-T). 2,3-pentadienal then forms 1-butyne and 1,2-butadiene releasing CO. 1-butyne eventually forms C_4H_4 radical and 1-2-butadiene forms benzene both of which adds to soot formation. Methylfuran also releases a methyl radical by reaction with H atoms to form furan or 1,3-butadien-1-one which eventually forms C_3H_4-P, C_3H_5-A, C_3H_3, C_2H_4 or C_2H_2. Each of the species formed eventually enable pathways to benzene, and subsequently more PAHs, via the previously illustrated example to form. These reaction pathways can explain the higher SY_E realized in experiments shown in Fig. 6 after 2. From Fig. S3, it can also be observed that there are several pathways which enable the formation of carbon monoxide leading credibility that the O in methylfuran may readily lead to the formation of CO. This will result in a soot reduction effect for methyl furan as one carbon atom from biofuel molecule escapes as CO and does not contribute to soot growth. Explaining why less soot is observed before 2000μs in Fig. 6.

Diisobutylene

Within Fig. S4, the reaction pathway for α-diisobutylene oxidation is presented at an equivalence ratio of 8.6. As expected, the most dominant two reactions involve unimolecular decomposition releasing either: a CH_3 to form 2,4-dimethylpentenyl; or dissociating into tertiary butyl radical (TC_4H_9) and 2-methyl propenyl radical (IC_4H_7). Formation of C_3H_5-T, C_3H_4-A, C_3H_3 and CH_3 are likely through the former pathway; while conversely the latter forms methyl radicals and C_3H_6. All of these species will then follow the pathway shown in baseline case Fig. S2 to form PAHs which result in increased soot production. H abstraction pathway by H atoms also plays a significant role in diisobutylene oxidation at high equivalence ratios. These reactions as shown in Fig. S4 form more of C_3H_4-A and CH_3 radicals which contributes to PAH growth as shown in Figs. S1 and S2 Illustrated reaction pathways can explain the SY_E increase over baseline found in experiments shown in Fig. 7.

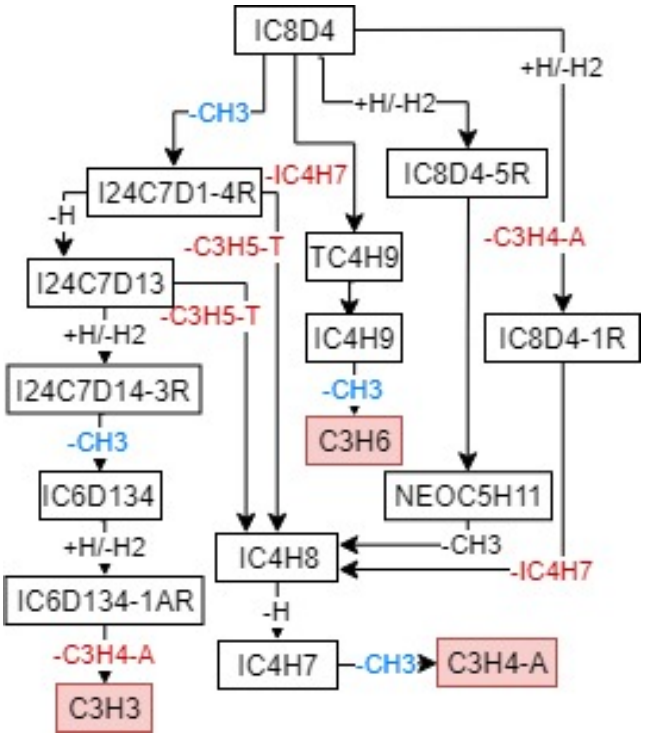

Figure S4. Reaction pathway for diisobutylene at 1850K and 4.5 atm showing dominant reactions. Refer to the color version of this figure.

Ethanol

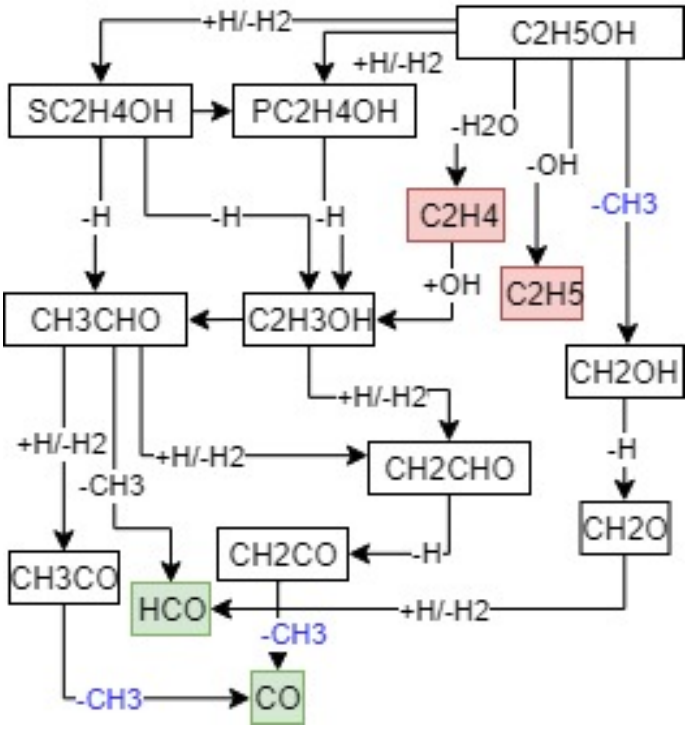

Figure S5. Reaction pathway for ethanol at 1850K and 4.5 atm showing dominant reactions. Refer to the color version of this figure.

An investigation of the major reaction pathway in ethanol blend at this rich equivalence shows that ethanol readily undergoes unimolecular decomposition into CH_2OH, C_2H_5 and C_2H_4 by releasing CH_3, OH and H_2O (Fig. S5) at high temperatures. While C_2H_5 and C_2H_4 follow the pathway shown in the baseline case (Fig. S1) for their growth to PAHs, CH_2OH forms CO after forming HCO. The CH_2OH reaction pathway can explain the SY_E reduction realized in experiments shown in Fig. 7. The H-abstraction pathways to SC_2H_4OH and PC_2H_4OH are relatively slow compared to the unimolecular decomposition pathways. The decomposition of ethanol to CH_2OH and CH_3 creates more CH_3 radicals as compared to the baseline case which react with C_2H_3 (formed from ethylene in the mixture) to form C_3H_5-A and eventually C_3H_3 as shown in reactions below:

$$C_2H_3+CH_3 \Leftrightarrow C_3H_5\text{-}A+H$$
$$C_3H_5\text{-}A \Leftrightarrow C_3H_4\text{-}A + H$$
$$C_3H_4\text{-}A+H \Leftrightarrow C_3H_4\text{-}P+H$$
$$C_3H_4\text{-}P+H \Leftrightarrow C_3H_3+H_2$$

This pathway will result in more PAH and eventually adds up to soot. Hence, in the present state, the Co-Optima mechanism predicts more soot from ethanol than baseline as shown in Fig. 8. Nevertheless, the intended use of Co-Optima mechanism is not for predicting soot from combustion but to predict major combustion species and ignition delay of the biofuels.

Cyclopentanone

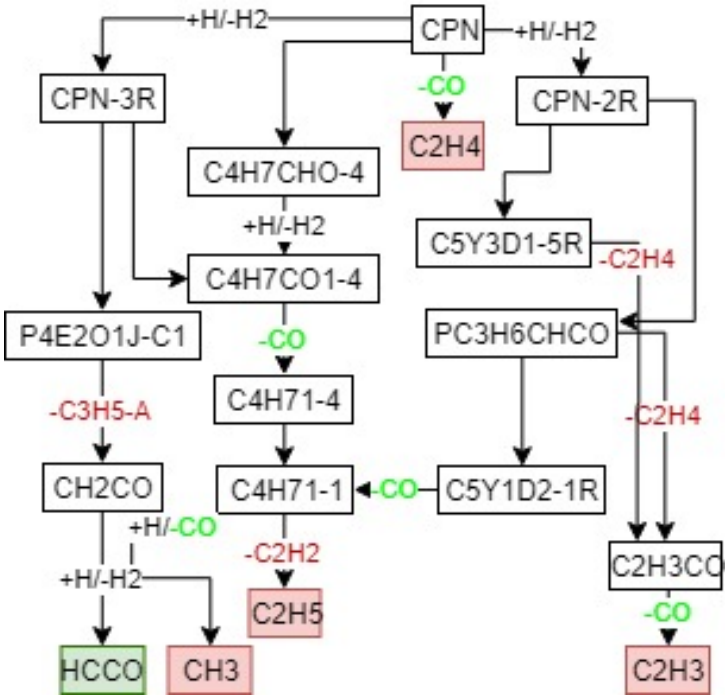

Figure S6. Reaction pathway for cyclopentanone at 1850K and 4.5 atm. Refer to the color version of this figure.

Figure S6 displays important pathways for cyclopentanone oxidation at high temperature and equivalence ratio of 8.6. For cyclopentanone, most dominant pathway is its decomposition into carbon monoxide and two ethylene molecules. Around 80% of initial decomposition of cyclopentanone follows this pathway. This reaction pathway can explain the SY_E reduction relative to baseline realized in experiments shown in Fig. 7 as significant amount of carbon content escapes as CO. Ethylene formed then follows the pathway shown in Fig. 10 to grow into benzene and larger PAHs. Other important pathways include H abstraction reactions to form cyclopentanone radicals CPN-3R and CPN-2R. These radical then undergoes further reactions to form C_3H_5-A, C_2H_4, C_2H_3, C_2H_2 and CH_3 radicals in the end. All these species contribute to PAH growth and to soot formation.

Methyl Acetate

Figure S7 shows the important reaction pathways for methyl acetate, which undergoes the following unimolecular decomposition at high temperature and equivalence ratio of 8.6:

$$CH_3COOCH_3 \Leftrightarrow CH_3CO_2 + CH_3$$
$$CH_3COOCH_3 \Leftrightarrow CH_3OCO + CH_3$$
$$CH_3COOCH_3 \Leftrightarrow CH_2CO + CH_3OH$$

The first two reactions release methyl radicals which contributes to PAH growth as shown in Fig. S2. CH_2CO and CH_3OH formed from the third reaction undergoes further reactions to release CH_3 radical and CO. CH_3CO_2 and CH_3OCO then dissociates to form methyl radicals as shown below:

$$CH_3CO_2 \Leftrightarrow CH_3 + CO_2$$
$$CH_3OCO \Leftrightarrow CH_3 + CO_2$$

Along with methyl radical, CO_2 is released showing that both oxygen atoms present in methyl acetate escapes along with one carbon atom. This reaction pathway can explain the SY_E reduction realized in experiments compared to baseline shown in Fig. 7. Methyl radicals released in several steps are the main contributors to PAH and soot formation (through pathway presented in Fig. S1) in case of methyl acetate.

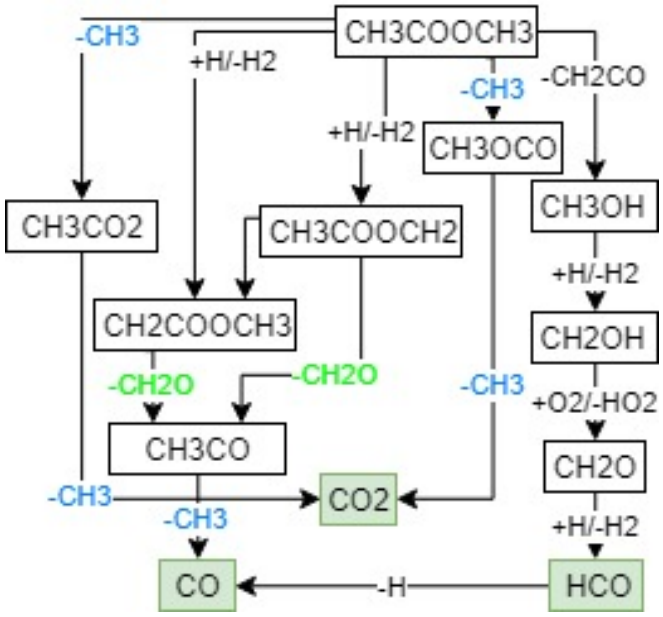

Figure S7. Reaction pathway for methyl acetate at 1850K and 4.5 atm. Refer to the colored version of this figure.

The following tables are the experimental data. With the temperatures and pressures provided, the induction time and soot yield for the mixtures are given. The uncertainty in the temperature is 2.0%, pressure is 1.8%, SY_E is 10%, and induction time is 0.5 μs.

Temperature (K)	Pressure (atm)	SY_E	Induction Time (μs)
1755	4.47	0.0010	2222
1772	4.39	0.0023	1899
1818	4.45	0.0065	1499
1846	4.51	0.0111	1286
1889	4.11	0.0165	927
1934	4.28	0.0205	556
1951	4.25	0.0181	554
2003	4.13	0.0096	474
2109	4.11	0.0041	202
2081	3.99	0.0033	153
2180	4.07	0.0039	46

Table S.1: The soot yield and induction time for each experiment of mixture 1, ϕ = 10.

Temperature (K)	Pressure (atm)	SY_E	Induction Time (μs)
1693	4.75	0.0007	2662
1750	4.72	0.0040	1700
1786	4.61	0.0100	1104
1853	4.54	0.0184	640
1921	4.47	0.0180	461
1989	4.37	0.0090	223
2052	4.22	0.0043	256

Table S.2: The soot yield and induction time for each experiment of mixture 2, the baseline mixture.

Temperature (K)	Pressure (atm)	SY_E	Induction Time (μs)
1726	4.72	0.0019	2044
1760	4.66	0.0052	1543
1793	4.56	0.0102	1345
1828	4.45	0.0162	889
1832	4.37	0.0165	861
1892	4.32	0.0189	553
1939	4.34	0.0160	387
1927	4.16	0.0147	367
1974	4.22	0.0118	334
2016	4.06	0.0041	190
2054	4.09	0.0044	156
2016	4.31	0.0077	123

Table S.3: The soot yield and induction time for each experiment of mixture 3, methyl furan.

Mixture 4

Temperature (K)	Pressure (atm)	SY_E	Induction Time (μs)
1757	4.62	0.0031	1780
1798	4.50	0.0099	1406
1823	4.54	0.0172	997
1843	4.58	0.0208	948
1852	4.55	0.0235	868
1872	4.47	0.0230	755
1898	4.28	0.0231	590
1953	4.40	0.0188	268
1961	4.35	0.0164	238
2003	4.28	0.0111	232
2050	4.18	0.0066	223
2107	4.12	0.0030	120

Table S.4: The soot yield and induction time for each experiment of mixture 4, Diisobutylene.

Temperature (K)	Pressure (atm)	SY_E	Induction Time (μs)
1769	4.59	0.00288	1485
1770	4.49	0.0039	1477
1816	4.56	0.0081	1102
1834	4.63	0.0105	840
1836	4.42	0.0102	793
1890	4.34	0.0088	510
1936	4.37	0.0065	438
1978	4.37	0.0048	288
1983	4.25	0.0037	265
1988	4.20	0.0019	217

Table S.5: The soot yield and induction time for each experiment of mixture 5, ethanol.

Temperature (K)	Pressure (atm)	SY_E	Induction Time (μs)
1776	4.53	0.0033	1748
1798	4.39	0.0045	1492
1847	4.36	0.0122	979
1880	4.37	0.0149	724
1926	4.39	0.0134	409
1971	4.29	0.0089	380
2024	4.64	0.0038	184

Table S.6: The soot yield and induction time for each experiment of mixture 6, cyclopentanone.

Temperature (K)	Pressure (atm)	SY_E	Induction Time (μs)
1761	4.46	0.0012	1758
1808	4.42	0.0052	1277
1844	4.49	0.0150	1046
1878	4.47	0.0145	612
1880	4.57	0.0156	593
1919	4.43	0.0113	555
1965	4.33	0.0077	294
2005	4.29	0.0043	180
2041	4.40	0.0026	101

Table S.7. The soot yield and induction time for each experiment of mixture 7, methyl acetate.

References

1. G. L. Agafonov *et al.*, Soot formation during the pyrolysis and oxidation of acetylene and ethylene in shock waves. *Kinetics and Catalysis* **56**, 12-30 (2015).
2. G. L. Agafonov *et al.*, Soot Formation During Pyrolysis of Methane and Rich Methane/Oxygen Mixtures Behind Reflected Shock Waves. *Combustion Science and Technology* **180**, 1876-1899 (2008).
3. Z. Hong, D. F. Davidson, S. S. Vasu, R. K. Hanson, The effect of oxygenates on soot formation in rich heptane mixtures: A shock tube study. *Fuel* **88**, 1901-1906 (2009).
4. U. Kc, M. Beshir, A. Farooq, Simultaneous measurements of acetylene and soot during the pyrolysis of ethylene and benzene in a shock tube. *Proceedings of the Combustion Institute* **36**, 833-840 (2017).
5. K. Johansson, M. Head-Gordon, P. Schrader, K. Wilson, H. J. S. Michelsen, Resonance-stabilized hydrocarbon-radical chain reactions may explain soot inception and growth. **361**, 997-1000 (2018).
6. S. Sinha, R. K. Rahman, A. J. P. C. C. P. Raj, On the role of resonantly stabilized radicals in polycyclic aromatic hydrocarbon (PAH) formation: pyrene and fluoranthene formation from benzyl–indenyl addition. **19**, 19262-19278 (2017).